Available online at www.sciencedirect.com
SCIENCE DIRECT®
ELSEVIER
Nuclear Physics A 724 (2003) 455–476
NUCLEAR PHYSICS A
www.elsevier.com/locate/npe

Critical-like behaviours in central and peripheral collisions: a comparative analysis

M. D'Agostino [a,*], M. Bruno [a], F. Gulminelli [b], R. Bougault [b], F. Cannata [a], Ph. Chomaz [c], F. Gramegna [d], I. Iori [e], N. Le Neindre [a,c], G.V. Margagliotti [f], A. Moroni [e], G. Vannini [a], J.P. Wieleczko [c]

[a] *Dipartimento di Fisica and INFN, Bologna, Italy*
[b] *LPC Caen (IN2P3-CNRS/ISMRA et Université), F-14050 Caen cédex, France*
[c] *GANIL (DSM-CEA/IN2P3-CNRS), B.P. 5027, F-14021 Caen cédex, France*
[d] *INFN Laboratorio Nazionale di Legnaro, Italy*
[e] *Dipartimento di Fisica and INFN, Milano, Italy*
[f] *Dipartimento di Fisica and INFN, Trieste, Italy*

Received 18 March 2003; received in revised form 7 May 2003; accepted 13 May 2003

Abstract

Quasi-projectile events from peripheral 35 A MeV Au + Au collisions are compared with 25 A MeV Au + C, 25 and 35 A MeV Au + Cu and 35 A MeV Au + Au central events. By fitting the measured charge yields with the Fisher droplet model technique, all the different data sets coherently point to a value $E_c^* \approx 4.5$ A MeV as the excitation energy where size distribution are best fitted by a power law. The physical parameters extracted from the fit strongly depend on the detailed shape assumed for the scaling function with the exception of τ and σ which are consistent with the critical exponents of the liquid-gas phase transition. Possible implications concerning the observation of a phase transition in multifragmentation experiments are discussed.

PACS: 24.10.Pa; 64.60.Fr; 68.35.Rh

1. Introduction

Nuclear multifragmentation and its possible connection with a critical penomenon or a phase transition, has been the subject of intensive theoretical and experimental investigations.

* Corresponding author.
E-mail address: dagostino@bo.infn.it (M. D'Agostino).

0375-9474/03/$ – see front matter
doi:10.1016/S0375-9474(03)01541-0

Since the early 80's, size distributions have been fitted with power laws [1,2], and even more sophisticated critical analysis have been performed following theoretical concepts coming from percolation theory [2]. More recently an astonishingly good scaling behavior has been observed and a consistent set of critical exponents has been extracted from different sets of data [3,4]. Such a critical-like behavior has been tentatively associated to the critical point of the nuclear liquid-gas phase transition expected in nuclear matter [5] in the framework of the Fisher droplet model [1].

However, critical exponents and scale invariance are compatible with many different physical phenomena and not necessarily linked to a thermodynamic second order phase transition [6]. Even for systems presenting a phase transition belonging to the liquid-gas universality class, it has been recently shown [7] that clusters may exhibit signs of criticality also in the fluid region of the phase diagram, at temperatures and densities above the thermodynamical critical point.

To progress on this point, different experimental groups have tried to deduce thermodynamic quantities from data [8–10], leading to caloric curves and heat capacities that rather point to a first order phase transition.

These findings may be compatible with the observed signals of critical behaviors since in different statistical models size distributions that mimic a scale invariant behavior are observed inside the coexistence zone of very small systems [11–14]. At variance with critical behaviors at supercritical density [7], these scalings do not survive at the thermodynamic limit and are only artifacts of the finite size constraints [11–13].

From the nuclear physics point of view such a situation cannot be distinguished from a true critical behavior since experimentally the thermodynamic limit cannot be accessed, nuclear systems being limited to a few hundred of nucleons. Therefore, the observation of a scaling behavior in multifragmentation data can never prove that a genuine critical point has been explored and even less that such a point corresponds to the second order phase transition of the nuclear liquid gas phase diagram. For this reason throughout this paper we will systematically refer to the signs of scale invariance in the data as to *critical-like behaviors*.

In a recent analysis of Isis and EOS data [15], the Fisher droplet model has been used to reconstruct the coexistence region. It was assumed that the good quality of the Fisher scaling fit demonstrates the occurrence of a liquid-gas phase transition with a power law mass distribution only at the thermodynamic critical point; the low value of the corresponding energy observed experimentally was attributed to a finite size effect. This assumption is not consistent with the theoretical results mentioned above [7,11–14].

To add to the confusion, not all data [16–18] show critical-like behaviours at excitation energies near to the one identified as critical in Refs. [3,4]. For example, an effective exponent $\tau \ll 2$, which is forbidden in the limit of infinite systems, has been observed in central Au + Au collisions [17]. A tentative explanation suggests that the Coulomb interaction would prevent heavily charged systems to attain statistical equilibrium and that the whole analysis in terms of a phase transition would be meaningless [16].

To contribute to this debate we present a wide set of data analyzed with different scaling techniques [15,19], with a source size ranging from about 200 to about 350 nucleons, to understand the possible Coulomb effects. This analysis includes Au quasi-projectile data

for which fluctuations studies have suggested a first order phase transition with negative heat capacity [9].

We will show that:

- in agreement with our previous findings [4] the different data sets point to the same values of the critical-like exponents τ, σ and of the critical-like excitation energy E_c^*; these values are robust with respect to possible effects induced by the Coulomb interaction and by the centrality of the reaction;
- the violation of scaling behaviors for heavy sources can in some cases be ascribed to different time scales in the deexcitation process;
- a comparable quality of scaling is obtained with very different prescriptions for the scaling function.

The fact that all the analyzed reactions behave as a universal multifragmentation process independent of the entrance channel and directly correlated with the available energy and mass only, is a strong indication of a microcanonical equilibrium. On the other hand, the invariance of the quality of the scaling with respect to the assumed shape of the scaling function means that scaling "per se" does not demonstrate the existence of a phase transition, and even less defines its order or allows to situate the system on the phase diagram; as a consequence it is not possible to extract the phase diagram from the parameters of the fit in a model independent way.

The plan of the paper is as follows. After a short presentation in Section 2 of the different data samples, the scaling properties of Au quasi-projectiles detected in peripheral collisions of the 35 A MeV Au + Au reaction will be reviewed in Section 3. The different central data sets are presented in Section 4 (where a correlation function technique is used to back-trace secondary fission) and analyzed in terms of Fisher scaling. Conclusions are drawn in Section 5.

2. Experiment

All the measurements presented in this paper have been performed at the K1200-NSCL cyclotron of the Michigan State University with the MULTICS-MINIBALL apparatus. Experimental details have been reported in Ref. [4]. Charged particles and fragments with charge up to $Z = 83$ were detected at $3^\circ \leqslant \theta_{\rm lab} < 25^\circ$ by the Multics array [20]. Charged particles and fragments of element number $Z \leqslant 20$ were detected at $25^\circ \leqslant \theta_{\rm lab} \leqslant 160^\circ$ by 171 phoswich detector elements of the MSU Miniball array [21]. The geometric acceptance of the combined array was larger than 87% of 4π. The charge identification thresholds in the Multics array were $E_{\rm th}/{\rm A} \approx 1.5$ MeV independent of the fragment charge, and $E_{\rm th}/{\rm A} \approx 2, 3, 4$ MeV for $Z = 3, 10, 18$, respectively, in the Miniball.

Peripheral collisions of a predominantly binary character have been selected for the reaction Au + Au at 35 A MeV [4]. A quasi-projectile source of nearly constant charge and excitation energy from 1 to about 8 A MeV was reconstructed via an event shape analysis. The fragment angular distributions [9] are compatible with an isotropic emission. The

reproduction of the experimental charge partitions by statistical model calculations [22] is consistent with a good degree of source equilibration [4,23].

For the reactions Au + Cu at 25 and 35 A MeV the most central 10% of the total measured cross section has been selected by a charged particle multiplicity cut. Well detected events (total detected charge larger than 90% of the total charge) have been analyzed in terms of event shape and the selected almost spherical events ($\Theta_{\text{flow}} \geqslant 60^\circ$) are hereafter presented. The same procedure has been followed to select central events in the 35 A MeV Au + Au reaction, while in the Au + C collision at 25 A MeV the average fragment multiplicity $\langle M \rangle = 2.2$ (standard deviation 0.2) is too low to perform any shape analysis and only the total multiplicity and total detected charge criteria have been applied.

The excitation energy of the emitting sources has been determined by calorimetry on an event by event basis, summing up the kinetic energies of all products in the source reference frame, taking into account the mass balance and correcting for the undetected neutrons [4]. This allows a sorting of the events as a function of energy as in the microcanonical statistical ensemble.

Mass numbers for clusters of charge 1 and 2 were measured. To determine the mass distribution, clusters of a given charge Z have been counted on an event by event basis and it has been assumed that the mass multiplicities $N(A)$ are equal to $N(Z)$. Checks have been made on the influence of the mass estimation. Our main conclusions do not change if we estimate the cluster mass from the mass to charge ratio of the fragmenting system or we assume the mass of stable nuclei.

3. QP source: scaling of static observables

3.1. RG scaling

Renormalization group (RG) arguments lead to the expectation of finite size scaling on different physical quantities (correlation length, susceptibility, heat capacity…) close to a second order phase transition point [24]. Inspired by the Fisher model, Stauffer and Aahrony [19] have proposed that the same scaling ansatz may apply to the cluster size distribution

$$n(A,\epsilon) = q\,A^{-\tau} f\left(\epsilon A^{\sigma}\right), \tag{1}$$

where $n(A,\epsilon) = N(A,\epsilon)/A_0$ is the cluster distribution normalized to the size of the fragmenting system, q is a normalization constant depending solely on τ [19,25], f is the scaling function, τ, σ are universal critical exponents and $\epsilon = (E^*_c - E^*)/E^*_c$ measures the distance from the critical point of events sorted as a function of the excitation energy E^* of the system.

In particular, percolation data are very well described by this ansatz [19]; this shows that Eq. (1) can hold in a large variety of physical situations not necessarily connected to a thermodynamic transition.

For peripheral Au + Au collisions the critical-like exponents as well as the critical-like excitation energy of the quasi-projectile source (QP) were extracted from the analysis of the moments of the charge distribution [4]. The critical-like exponents ($\tau = 2.12, \sigma = 0.64$)

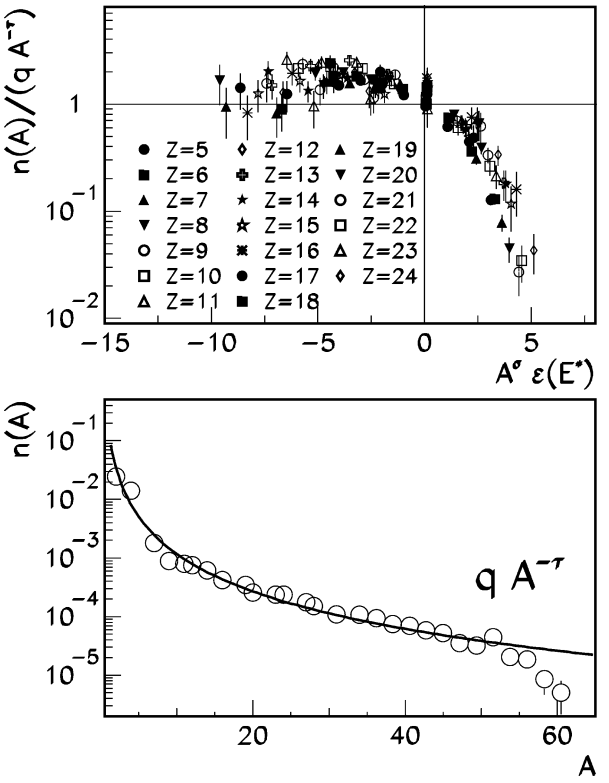

Fig. 1. Peripheral Au + Au collisions. Top panel: scaling function for the QP source with the ansatz of Eq. (1). Bottom panel: mass distribution of the QP decay products in the range $4 \leqslant E^* \leqslant 5$ A MeV, solid line: power law with $\tau = 2.12$ [4].

form a consistent set and are close to the values of the liquid-gas universality class. Near the excitation energy identified as "critical" from the behavior of the largest fragment [4], $E_c^* \approx 4.5$ A MeV, the size distribution is well described by a power law of exponent $\tau = 2.12$ as shown in the bottom panel of Fig. 1.

By applying Eq. (1) to the QP events, a scaling behavior is observed (Fig. 1 top panel) over the whole range of excitation energy and fragment charge $Z \geqslant 5$. Since for the lightest fragments side feeding due to the primary fragments decay or non-equilibrium effects could affect the final production rate, fragments with $Z < 5$ were disregarded.

3.2. Fisher scaling

In recent papers [15,25] Elliott et al. analyze the critical behavior of the size distribution in terms of the Fisher droplet model. In this model [26] the vapor coexisting with a liquid in the mixed phase of a liquid-gas phase transition is described by an ideal gas of clusters.

A scaling around the critical point, similar to Eq. (1) is assumed, but a different form is suggested for the scaling function

$$n(A,T) = qA^{-\tau}\exp\left(\frac{\Delta G(A,T)}{T}\right), \tag{2}$$

where $\Delta G(A,T)$ represents the variation of the Gibbs free energy upon formation of a drop of A nucleons out of an homogeneous nuclear vapor at temperature T

$$\Delta G(A,T) = A\Delta\mu - c_0\epsilon A^{\sigma}. \tag{3}$$

$\Delta\mu = \mu - \mu_{\mathrm{coex}}$, where μ is the chemical potential of the system and μ_{coex} the chemical potential at coexistence. σ is a critical exponent related to the ratio of the surface to volume dimension, $\epsilon = (T_c - T)/T_c$ measures the distance from the critical point, and c_0 is the surface energy coefficient. This expression can be extended to charged systems [27] by calculating [22] the Coulomb part of the free energy δC in the Wigner–Seitz approximation

$$\Delta G_{\mathrm{tot}}(A,Z,T) = \Delta G(A,T) - \delta C = \Delta G(A,T) - \frac{3}{5}e^2\frac{Z^2}{R}\left[1 - \left(1 - c_c\epsilon^{\beta}\right)^{1/3}\right], \tag{4}$$

where R is the radius of a fragment of mass A, c_c is a parameter related to the density of the liquid phase [27], and β is a critical exponent.

For sake of simplicity and to perform a direct and quantitative comparison among different sets of data, the analysis hereafter presented has been performed with the same estimate of T as in Ref. [15], i.e., $T = \sqrt{8E^*}$. The influence of the estimate of T on the results has also been considered (see below).

In principle $\Delta\mu$ as well as c_0 [15] and c_c can depend on the excitation energy. To avoid an uncontrolled proliferation of fitting parameters we have taken the simplest parameterization that allows a good quality fit of the whole cluster size distribution: c_0 and c_c have been treated as constants and the exponent β has been fixed at the value $1/3$ as resulted from a previous analysis on the same source [4].

It is important to remark that Eqs. (2)–(4) give an oversimplified description that does not take into account finite fragment size effects. A more sophisticated droplet model, incorporating thermodynamically consistent excluded volume effects has been recently proposed in Ref. [28].

By using the ansatz Eqs. (2)–(4) we have performed a multi-parameter fit of the QP data (over 200 data points). The values of the parameters obtained from the fit are reported in Table 1 for two different prescriptions for $\Delta\mu$ (a constant value or a second order polynomial in E^*) together with some results obtained switching on/off the Coulomb term of Eq. (4).

Whatever parameterization is chosen for $\Delta\mu$, its value at $E^* = E_c^*$ is compatible with zero within the errors, which correspond to a 99% confidence level. This demonstrates that the best fit of the charge distribution around $E^* \approx E_c^*$ (see Fig. 1, lower part) is indeed given by a power law. Checks were also made on the parameterization chosen for the Coulomb term. Results compatible with those reported in Table 1 are obtained with the parameterization used in Ref. [15].

Table 1
Values of the critical-like exponents τ, σ, critical-like excitation energy E_c^*, "surface energy" coefficient c_0, $\Delta\mu$ at $E^* = E_c^*$ and χ^2 of the Fisher scaling fit through Eqs. (2)–(4)

Peripheral collisions	τ	σ	E_c^* (A MeV)	c_0	$\Delta\mu(E_c^*)$ (A MeV)	χ^2
$\delta C = 0$, $\Delta\mu = 0$	2.05 ± 0.01	0.66 ± 0.06	4.19 ± 0.06	3.3 ± 0.6	–	1.5
$\delta C = 0$, $\Delta\mu = \text{const}$	2.07 ± 0.02	0.70 ± 0.03	4.5 ± 0.4	3.0 ± 0.3	0.0 ± 0.1	1.6
$\delta C = 0$, $\Delta\mu = f(E^*)$	2.10 ± 0.02	0.66 ± 0.02	4.5 ± 0.1	8.0 ± 0.3	0.0 ± 0.2	1.3
δC Eq. (4), $\Delta\mu = f(E^*)$	2.08 ± 0.02	0.66 ± 0.02	4.40 ± 0.05	10.9 ± 0.4	0.1 ± 0.1	1.7

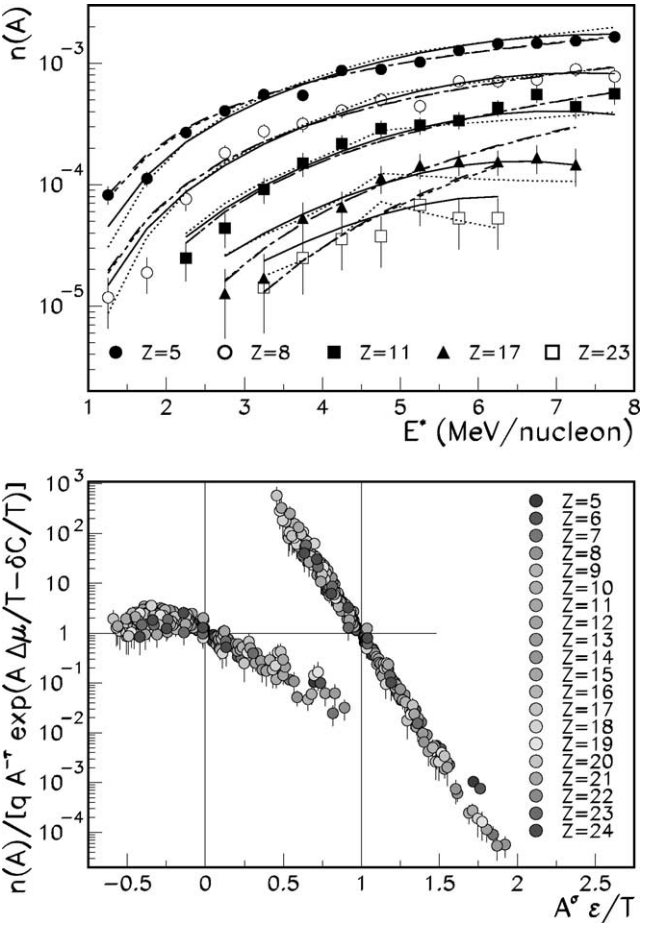

Fig. 2. Top panel: cluster yields of the QP source as a function of the excitation energy (symbols) and fits with Eq. (2). Dotted line: δC Eq. (4) and $\Delta\mu = f(E^*)$, solid line: $\delta C = 0$ and $\Delta\mu = f(E^*)$, short dashed line: $\delta C = 0$, $\Delta\mu = 0$, long dashed line: $\delta C = 0$, $\Delta\mu = \text{const}$. Bottom panel: scaled yield distribution versus the scaled T for the cases: $\delta C = 0$, $\Delta\mu = 0$ (left) and $\Delta\mu = f(E^*)$ (right). To represent the results on the same picture a constant horizontal shift $C = 1$ is applied to the latter distribution.

3.3. Robustness of the fitting procedure

The Fisher fit produces a scaling behavior for the data comparable to the RG ansatz, as can be seen in Fig. 2 (bottom panel). Critical-like exponents and the critical-like excitation energy, reported in Table 1, are in agreement with the previous analyses [4]. The similarity of the results obtained with the RG and with the Fisher scaling demonstrates that the values of the critical-like parameters are very robust with respect to the detailed shape assumed for the scaling function. On the other hand this also implies that the adequacy of the Fisher ansatz to describe the data is not a sufficient condition to give any detailed physical meaning to the values of the fit parameters $\Delta\mu$, c_0, c_c. E.g., the quality of the fit and the value of the exponents do not drastically change if one suppresses the Coulomb as well as the $\Delta\mu$ term [25] (see Table 1); however, the value of c_0 strongly depends on the parameterization of the scaling function. Fig. 2 shows that depending on the choice made for $\Delta\mu$ on can observe a scaling of the yields over seven or only two orders of magnitude. This clearly shows that the adequacy of the fit cannot be measured by the full scale of the scaled yields. It is also interesting to remark that, similarly to the RG ansatz, the scaling obtained with the Fisher scaling function is observed in the subcritical as well as in the overcritical domain [29,30] even if in the context of the Fisher model Eq. (2) has no physical meaning for $E^* > E_c^*$. This is more quantitatively shown in Fig. 2 (top panel) which compares the measured production yields of a few clusters with the results of the fit. As already observed in Ref. [30] a parameterization $\Delta\mu = f(E^*)$ allows the Fisher scaling function to reproduce the data well above the critical excitation energy. On the contrary, when $\Delta\mu$ is treated as a constant, the reproduction of large clusters yields is satisfactory only up to the critical-like excitation energy and scaling is observed (bottom panel) only up to the critical excitation energy. This is again an indication that the astonishingly good quality of the scaling may come from a physical phenomenon more general than that described by the Fisher model.

One may also wonder what physical meaning can be attributed to a Fermi gas estimator of the temperature at excitation energies of several A MeV. Indeed, for this experimental sample the temperature evaluated from an isotope [23] and a kinetic energy thermometer [9] strongly deviates from the Fermi gas ansatz as shown in the left part of Fig. 3. If we use a polynomial fit of the measured temperature (full line in Fig. 3) as an ansatz for the T parameter in the Fisher fit, the quality of the scaling (shown in the right part of Fig. 3) is not modified, nor the extracted values for τ, σ, c_0. The only effect of the more sophisticated caloric curve is that the energy domain compatible with $\Delta\mu = 0$, i.e., with a power law for the fragment yield, is stretched to the domain $4.25 < E_c^* < 4.75$ A MeV. Once again this shows that the value of the critical-like quantities is robust respect to the different parameterizations for the scaling function, while it is certainly hazardous to attribute a physical meaning to the thermodynamical parameters and extract a direct relation to the equation of state of nuclear matter based on the quality of the scaling.

In order to validate a Fisher scaling analysis for data sets such as central collisions, where the excitation energy distribution is narrow, the fitting procedure has also been performed on reduced samples of QP events in small excitation energy intervals. The results are summarized in Table 2.

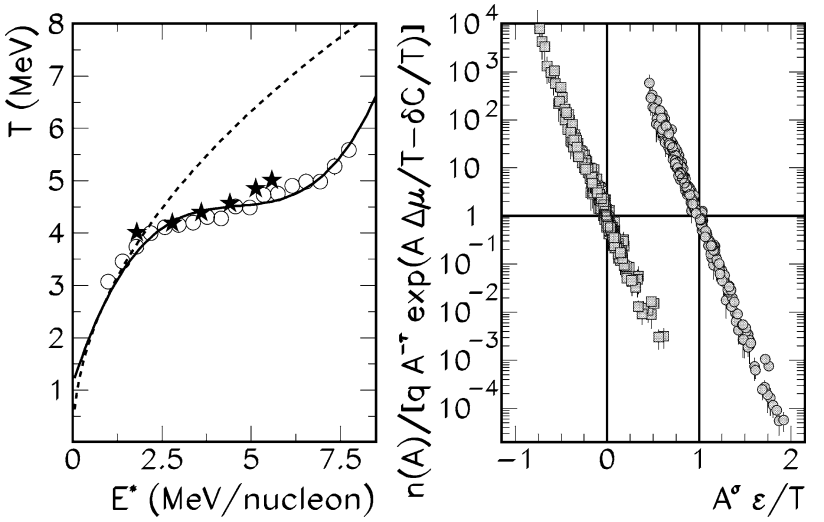

Fig. 3. Left side: different estimations of the QP source temperature. Circles: kinetic energy thermometer from Ref. [9]. Solid line: fit of the previous point with a third order polynomial. Stars: isotopic thermometer from Ref. [23]. Dashed line: Fermi gas ansatz $\sqrt{8E^*}$. Right side: scaled yield distribution as a function of the scaled T. Squares: same as in Fig. 2 above (T is estimated from the solid line of the left panel). Circles: same as squares, but T is estimated from the dashed line of the left panel). To represent the results on the same picture a constant horizontal shift $C = 1$ is applied to the latter distribution.

Table 2
Values of the critical-like exponents τ, σ, critical-like excitation energy E_c^*, "surface energy" coefficient c_0, $\Delta\mu$ at $E^* = E_c^*$ and χ^2 of the Fisher scaling fit through Eqs. (2)–(4) in bins of excitation energy

Peripheral collisions	τ	σ	E_c^* (A MeV)	c_0	$\Delta\mu(E_c^*)$ (A MeV)	χ^2
$E^* = 1$–2 (A MeV)	2.5 ± 0.2	0.66 ± 0.03	4.5 ± 0.6	10.0 ± 0.7	-7.0 ± 3.0	1.4
$E^* = 2$–3 (A MeV)	2.1 ± 0.1	0.65 ± 0.03	4.5 ± 0.3	10.0 ± 0.9	-0.2 ± 0.8	1.0
$E^* = 3$–4 (A MeV)	2.10 ± 0.08	0.68 ± 0.05	4.5 ± 0.2	10.0 ± 1.5	0.0 ± 0.5	0.7
$E^* = 4$–5 (A MeV)	2.08 ± 0.04	0.66 ± 0.02	4.5 ± 0.2	10.0 ± 5.0	0.1 ± 0.2	1.0
$E^* = 5$–6 (A MeV)	2.08 ± 0.02	0.66 ± 0.06	4.50 ± 0.02	10.1 ± 0.2	-0.04 ± 0.03	1.1
$E^* = 6$–7 (A MeV)	2.08 ± 0.02	0.66 ± 0.04	4.50 ± 0.02	10.1 ± 0.1	-0.01 ± 0.03	1.5
$E^* \geqslant 7$ (A MeV)	2.08 ± 0.02	0.66 ± 0.03	4.46 ± 0.02	10.0 ± 0.1	-0.13 ± 0.03	1.1

As it can be seen in Table 2, for all energy intervals by the fitting procedure one obtains the same critical-like energy even when this latter lies outside the considered bin. The critical-like exponents are in agreement with those shown in Table 1.

The uncertainties in the critical-like exponents and in the critical-like excitation energy decrease with increasing E^*, signaling that only an approximate description of the critical region can be provided by events in the low energy regime, as it has previously found [30] for Lattice Gas events. The large uncertainties of the fit when the critical-like energy is far from the fitting interval is also indicated by the value of $\Delta\mu$ calculated at E_c^*. While this value is compatible with zero for all the excitation energy bins $E^* > 2$ A MeV, this is

not the case for the first interval of excitation energy. A small deviation from zero is also present in the highest energy interval.

To conclude this section, we have shown that the Fisher scaling technique leads to an estimation of the critical-like exponents and the critical-like excitation energy that does not depend on the details of the technical implementation of the fitting procedure. However, the adequacy of the Fisher ansatz to the data is not sufficient to give a physical meaning to the other fit parameters, thus it does not allow to extract any direct information on the phase diagram.

4. Central collisions

4.1. Equilibration

We have shown in the previous section that a critical-like behavior is clearly observed around $E_c^* = 4.5$ A MeV for QP events. Independently of the assumed parameterization of the scaled yields, fragment partitions corresponding to $E^* = E_c^*$ are recognized as power laws and only one functional form describes the fragmentation process in the whole range of excitation energies. To explore the effects of the entrance channel and/or the size of the system we will now turn to the analysis of central collisions.

We present here results for central collisions measured in the reactions Au + C at 25 A MeV incident energy, Au + Cu at 25 A MeV, 35 A MeV and Au + Au at 35 A MeV.

First we show that the considered central events are compatible with the decay of equilibrated sources and, therefore, are good candidates for an analysis in terms of Fisher scaling.

Fig. 4 shows the correlation between the fragment charge and the velocity along the beam direction [31]. In this representation one can observe that the general trend for fragments is to be isotropically emitted. Their velocity is symmetrically distributed around zero, i.e., the considered sources are at rest in the center of mass frame.

In Fig. 5 we compare the measured charge distributions to statistical model predictions. The same normalization to the total number of events is applied to the experimental and calculated distributions, which thus can be compared on an absolute scale.

The Au + C data are the standard prototype of low energy compound nucleus deexcitation. Due to the strongly forward focused kinematics and to the minimum detection angle ($\theta_{\rm lab} > 3^\circ$), complete events are detected only in the case of fission of the compound. The charge distribution displayed in Fig. 5 (top panel) is well reproduced by the Gemini [32] code, which describes fragment production as a sequence of binary fission-like emissions. A similar degree of reproduction is also obtained with the SMM [22] model (see, for instance, Fig. 4 of Ref. [4]). The excitation energy needed to the models to reproduce the experimental distribution (1.4 A MeV) agrees with the experimental value.

The charge distribution of the central collisions extracted from the Au + Cu 25 and 35 A MeV reactions are compared to statistical SMM model calculations [22], where the mass of the fragmenting source has been assumed to be 90% of the total mass of the system. The model reproduces well the data with input excitation energies (3.3 and 4.1 A MeV

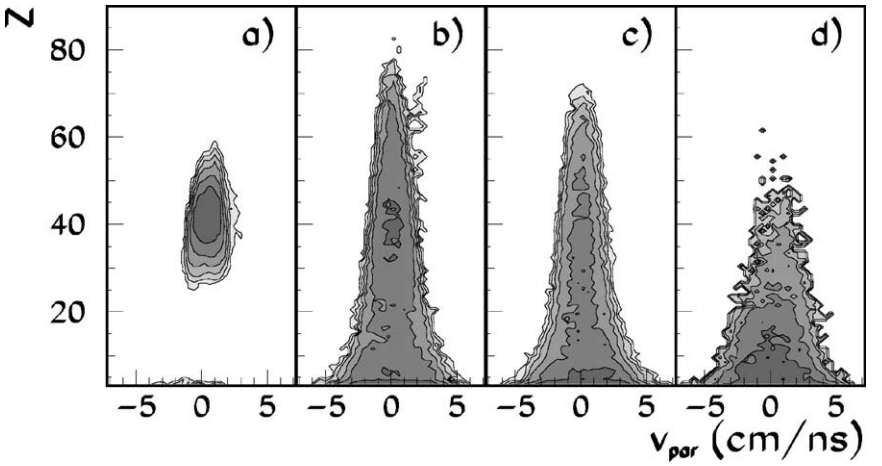

Fig. 4. Fragment charge Z versus the velocity component along the beam direction in the center of mass reference frame for central Au + C events at 25 A MeV (a), Au + Cu events at 25 (b) and 35 A MeV (c), and Au + Au central collisions at 35 A MeV (d).

for the 25 and 35 A MeV data, respectively) close to the average energies measured by calorimetry.

The decay of the Au + Au source (bottom panel of Fig. 5) is also very well described by the statistical SMM model [33–35]. At variance with the other reactions, a contribution of radial flow of about 1 A MeV seems to be superimposed to the thermal excitation. The freeze-out density of this system, evaluated from the backtracking of experimental data, is about 1/6 [34] of the normal density, lower than the densities of the other sources, which are estimated from the same model as about 1/3 of the normal density.

The same kind of agreement with statistical models is also observed, for all the considered reactions, for the charge partitions [33,34] as well as for the fragment kinetic energies. The close similarity between statistical models and data, together with the isotropy of fragment emission (see Fig. 4), suggest that these sets of data are close to a statistical equilibrium and can then be compared to the QP sample.

4.2. Fisher scaling

In the case of the 35 A MeV Au + Cu sample the excitation energy is close to the value where the QP shows critical-like partitions with $\tau \simeq 2$. However, as it appears from Fig. 5, the central events distribution is much flatter and can be approximately fitted only with an effective exponent $\tau_{\text{eff}} \simeq 1.4$. In the case of the 25 A MeV Au + Cu (35 A MeV Au + Au) the deposited energy is too low (too high) for expecting a critical-like behavior, however, the distributions are flatter than in the QP at comparable energy, with $\tau_{\text{eff}} \approx 1.4$ ($\tau_{\text{eff}} \approx 1.2$). The question naturally arises whether Coulomb or entrance channel effects have led the central collision fragmenting source through a different path in the phase diagram, and whether this can be recognized by studying the critical-like properties of the partitions. To this aim, the procedure adopted for the QP in Ref. [4] cannot be applied, since in these data

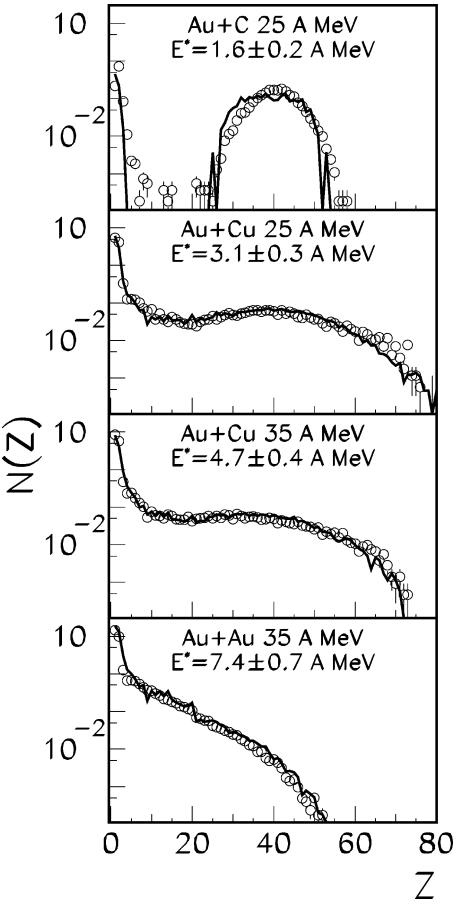

Fig. 5. Symbols: inclusive charge distributions for central Au + C events at 25 A MeV, Au + Cu at 25, 35 A MeV and Au + Au at 35 A MeV from top to bottom, respectively. The reported excitation energy and standard deviation are the experimental calorimetric values for each sample. Lines: filtered GEMINI (top panel) and SMM (other panels) predictions.

samples the excitation energy is distributed in a very narrow interval. However, we have shown in Section 3 that even for sets of data far from the critical-like excitation energy it is possible to get information on critical-like exponents by working with the Fisher scaling function.

The fitting procedure described in Section 3 has been applied to the four sets of data. The resulting scaling functions are shown in Fig. 6 and the corresponding parameters are reported in Table 3. All the data samples point to similar exponents and to the same critical-like energy, however, the situation is very different from the QP events. The values of the τ exponent are lower, the quality of the fit (evaluated through the χ^2) is far from being satisfactory and the values of $\Delta\mu$ at E_c^* are never compatible with zero.

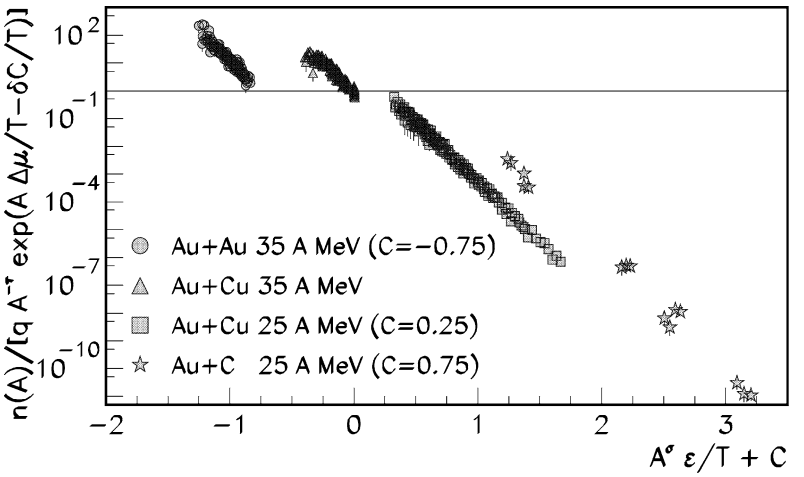

Fig. 6. Fit of central events with the scaling function ansatz of Eqs. (2)–(4). To represent the results on the same picture a constant horizontal shift C is applied to the distributions. Fragment charges range from 4 to 37.

Table 3
Values of the critical-like exponents τ, σ, critical-like excitation energy E_c^*, "surface energy" coefficient c_0, $\Delta\mu$ at $E^* = E_c^*$ and χ^2 of the Fisher scaling fit through Eqs. (2)–(4)

Central collisions	τ	σ	E_c^* (A MeV)	c_0	$\Delta\mu(E_c^*)$ (A MeV)	χ^2
Au + C 25 A MeV	1.8 ± 1.2	0.64 ± 0.02	4.39 ± 0.08	10.0 ± 0.1	2.7 ± 0.5	5.8
Au + Cu 25 A MeV	1.95 ± 0.01	0.74 ± 0.04	4.70 ± 0.04	10.0 ± 0.1	0.4 ± 0.1	1.6
Au + Cu 35 A MeV	1.97 ± 0.01	0.66 ± 0.02	4.36 ± 0.01	10.0 ± 0.5	0.23 ± 0.05	4.6
Au + Au 35 A MeV	2.05 ± 0.01	0.66 ± 0.01	4.45 ± 0.01	9.98 ± 0.06	0.22 ± 0.03	1.7

This is not very surprising in the case of the compound nucleus de-excitation events (Au + C reaction), where the measured excitation energy is very far from the critical-like one. The 35 A MeV Au + Cu reaction is more puzzling: the excitation energy domain contains the expected "critical" region, yet the high value of the χ^2 suggests a violation of the scaling, and the value of $\Delta\mu$ calculated at E_c^* is significantly non zero. This means that the effective $\tau_{\text{eff}} \simeq 1.4$ extracted from a simple two parameter fit of the charge distribution of Fig. 5 can in no way be interpreted as a critical exponent, in the sense that the charge distribution is never compatible with a power law in the Fisher framework. Fig. 6 also shows the ambiguities and dangers of the Fisher scaling technique. From the visual quality of the fit and the extracted critical-like parameters, we would have concluded that the Au + Cu sample was perfectly compatible with the QP one, while the simple observation of the charge distributions in comparable excitation energy domains (Figs. 1 and 5) clearly shows that this is not the case. Only a closer look at the χ^2 of the fit and on the value of $\Delta\mu$ allows to recognize that the Au + Cu sample is not compatible with a self-similar behaviour around a critical point as it would be suggested by the Fisher fit. This implies that the Fisher technique is a very helpful tool, but has to be complemented with other

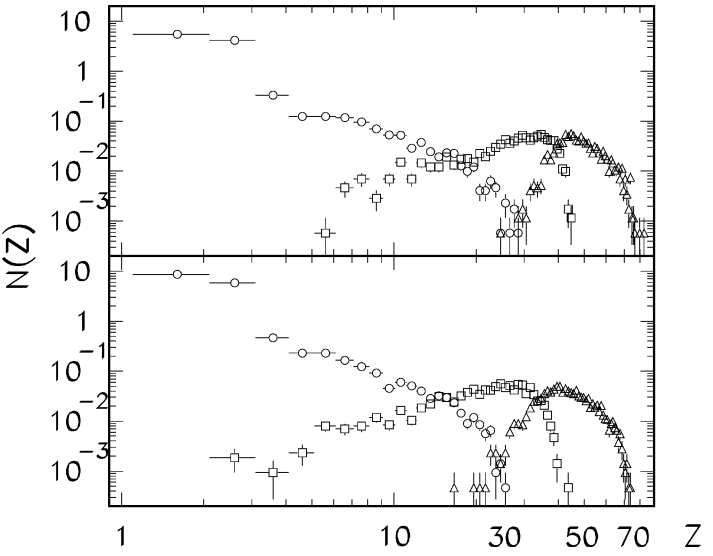

Fig. 7. Charge distribution of the largest fragment (triangles), the second largest (squares) and the remaining fragments (circles). Upper (lower) panel: central 25 (35) A MeV Au + Cu events.

analyses [4] before one can consider the effective linear behaviour shown in Fig. 6 as a universal scaling behaviour.

4.3. Identification of secondary fission

To thoroughly investigate the peculiar shape of the charge distribution for the Au + Cu system, we show in Fig. 7 the distribution of the largest, second largest and remaining fragments for the Au + Cu central collisions. The charge distribution of light fragments (circles) is steeper than the total distribution and the flattening, resulting in $\tau_{\text{eff}} \approx 1.4$, is mainly caused by the second largest fragment, whose distribution covers a wide charge range.

A possible interpretation of the tail observed towards small Z values of the second largest fragment is the possible increase of the secondary fission probability [36] for heavily charged systems. If this interpretation is correct, the two largest detected fragments are correlated by their mutual Coulomb repulsion and, in the asymptotic stage of the detection, a strong anticorrelation of their relative velocity, not smeared by the proximity of other fragments, should appear.

One can define [38,39] the two-fragment velocity correlation function as

$$1 + R(v_{\text{red}}) = C\frac{Y(v_{\text{red}})}{Y_{\text{back}}(v_{\text{red}})}, \tag{5}$$

where $v_{\text{red}} = (\vec{v}_i - \vec{v}_j)/\sqrt{(Z_i + Z_j)}$ is the reduced relative velocity of fragments i and j with charges Z_i and Z_j; $Y(v_{\text{red}})$ and $Y_{\text{back}}(v_{\text{red}})$ are the coincidence and background yields for fragment pairs of reduced velocity v_{red} and $C = N_{\text{back}}/N_{\text{coinc}}$ where N_{coinc} and

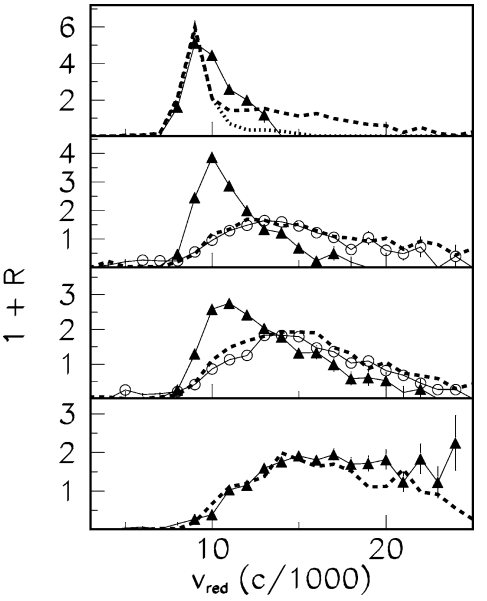

Fig. 8. Correlation functions of the reduced velocity for the two largest fragments in each event (triangles). From top to bottom: central Au + C events at 25 A MeV, Au + Cu at 25, 35 A MeV and Au + Au at 35 A MeV. Open symbols: the same correlation after re-clusterization (see text). Dashed lines: QP correlation at the same excitation energy as the corresponding central events.

N_{back} are the total number of coincidence and background pairs. The background yield is constructed by means of the mixed event technique [39].

Fig. 8 displays the correlation functions for all the sets of central events (triangles), compared to the QP events at the same excitation energy as the central sets (dashed lines).

For central Au + C events at 25 A MeV the correlation function is very similar to the QP one, especially when only fission events are considered (dotted line). The peak at $v_{\text{red}} \approx 10$ $(c/1000)$ corresponds to the reduced velocity of two touching charged spheres. This result shows that the velocity correlation function representation allows, also in a high multiplicity sample, to isolate clearly the ideal situation of a binary fission, where the two heaviest fragments are correlated by their mutual Coulomb repulsion independently of the other fragments, i.e., they are not produced at the freeze out stage but later [37].

Usually the correlation functions of the reduced velocity are compared with many-body trajectory calculations [38–40] to evaluate the fragment emission time. Here this observable is studied to compare the decay pattern of sources at the same excitation energy, but different in size. With this technique we do not try to establish the emission time but only to back-trace the binary Coulomb inter-fragment correlation; therefore, the spacetime ambiguity which is often associated to the correlation methods does not affect our results.

For central Au + Cu events the correlation function of the reduced velocity between the two heaviest fragments in each event signals a stronger correlation than in the QP decay at the same excitation energy. The Coulomb hole indeed is narrower than in the QP case and

the peak corresponding to the reduced velocity of two touching charged spheres, observed in the Au + C reaction, is still present even if the excitation energy of the source is larger.

For the Au + Au central collisions the correlation function (Fig. 8 bottom panel) does not give indications of secondary fission of the primary fragments. Whether the presence of flow influences the primary partitions or their secondary deexcitation, or a more sophisticated many-body correlation analysis [41] has to be performed, deserves further investigations.

The identification of a secondary fission contribution is an important step since in the Fisher scaling analysis, as well as in all reconstructions of the equation of state by statistical methods, primary fragment yields have in principle to be considered. If sequential evaporation is not expected to affect in a sizeable way the scaling properties and in general the critical-like observables [15], secondary fission can deform the production yields in an important way and data have to be corrected for this process. For the Au + Cu reactions one can use the correlation function information to back-trace the sequential emission. We reclusterize the two heaviest fragments with a Gaussian shaped probability distribution, centered at the Coulomb reduced velocity and with a width given by the left tail of the correlation function. When the two heaviest fragments are reclusterized, they are replaced in the event by a primary fragment with a charge equal to the sum of their charges and a velocity vector given by the weighted mean of their velocities. As shown in Fig. 8, after this procedure the correlation function has a very similar shape to the QP one in the same excitation energy range. This shows that the remaining fragments most likely come from an emission process with no specific time scale, i.e., compatible with a freeze out.

We may worry whether a reclusterization of the two heaviest fragments (when correlated with the Coulomb relative velocity) may suppress the multifragmentation channel with two fragments in the final state leading to a bias of the statistical ensemble. In this respect it is interesting to remark that in all samples most of the events where a secondary fission is recognized correspond to a fragment multiplicity equal to three, where a Coulomb peak in the velocity correlation unambiguously signs standard binary sequential decay [37].

4.4. Scaling analysis revisited

After the back-tracing of secondary fission the cluster size distribution for the central collisions Au + Cu at 25 and 35 A MeV are close to the QP size distributions at the same excitation energy (see Fig. 9).

In particular the 35 A MeV reaction follows a power-law with $\tau \approx 2$ as appears from the bottom panel of Fig. 9.

This means that, at least up to a source charge around 100, the increase of the Coulomb interaction seems to affect the decay of primary fragments, but not the bulk multifragmentation.

A power-law with exponent $\tau \approx 2$ corresponds to partitions with very large size fluctuations [42], as signaled by the Campi plot of the central events (Fig. 10), exhibiting both "liquid" as well "gas" branches.

A strong check of compatibility among QP events and Au + Cu central events consists in the finite size scaling of the moments of the size distribution.

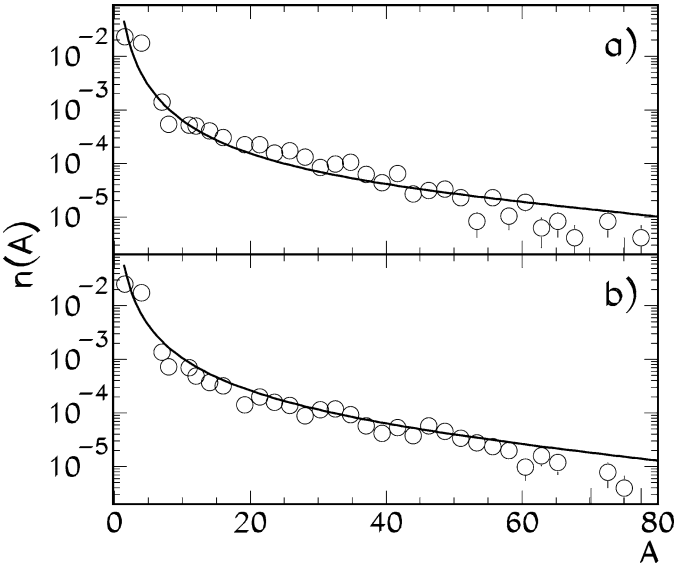

Fig. 9. Cluster size distribution for central Au + Cu events (open symbols), after reclusterization of the two heaviest fragments with the procedure described in the text. The line represents the power-law from Eqs. (2)–(4) describing the QP events at the same excitation energy as central Au + Cu 25 A MeV collisions (top panel) and Au + Cu 35 A MeV collisions (bottom panel).

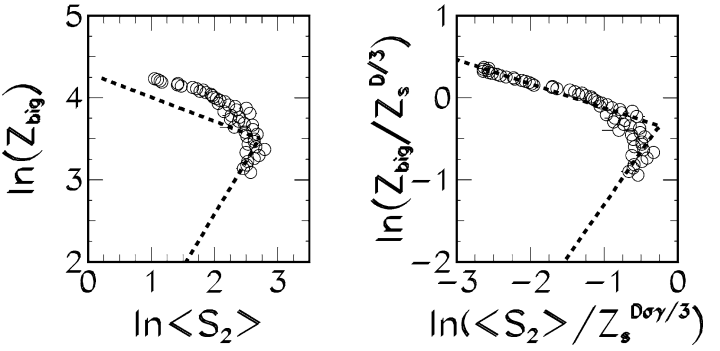

Fig. 10. Campi plot for the QP source (dashed line) and for 35 A MeV Au + Cu central collisions (symbols). In the left panel the unscaled distribution is given, in the right panel scaled moments are shown. Z_{big} and Z_S are the charge of the largest fragment and of the decaying source, respectively.

In Ref. [43] it has been shown that, as for percolation events, in finite nuclear systems near the critical-like excitation energy the size of the largest cluster and the second moment should scale for the size of the system following the hyper-scaling relation. The largest cluster size is expected to scale as $S^{D/3}$, where S is the size of the system, $D = \frac{d}{\tau-1}$ is the fractal dimension, $d = 3$ is the Euclidean dimension. The second moment S_2 is expected to scale as $S^{D\sigma\gamma/3}$, where $\gamma = (3-\tau)/\sigma$.

Table 4
Values of the critical-like exponents τ, σ, critical-like excitation energy E_c^*, "surface energy" coefficient c_0, $\Delta\mu$ at $E^* = E_c^*$ and χ^2 of the Fisher scaling fit through Eqs. (2)–(4)

Central collisions after reclusterization	τ	σ	E_c^* (A MeV)	c_0	$\Delta\mu(E_c^*)$ (A MeV)	χ^2
Au + Cu 25 A MeV	2.10 ± 0.04	0.60 ± 0.02	4.4 ± 0.1	10.0 ± 0.6	0.2 ± 0.2	1.8
Au + Cu 35 A MeV	2.05 ± 0.04	0.68 ± 0.03	4.5 ± 0.2	9.0 ± 1.0	0.1 ± 0.1	1.3
All central	2.05 ± 0.02	0.66 ± 0.02	4.40 ± 0.03	13.0 ± 0.4	0.1 ± 0.1	1.9

In the right panel of Fig. 10 the correlation between the charge of the largest fragment and the average second moment is shown for the central source, scaled [43] via the critical-like exponents of the QP source [4]. The observed agreement shows again the validity of the scaling [44] and the compatibility of critical-like exponents for the two systems. The same conclusion can be drawn from the Fisher scaling reported in Table 4. If the asymptotic yields are corrected for secondary fission, the quality of the scaling improves, the parameters (for a given guess of the scaling function) are still compatible with the QP ones, and $\Delta\mu$ is compatible with zero at $E^* = E_c^*$, i.e., the τ exponent observed in Fig. 9 is a genuine signal of a power law behaviour.

The fact that these two very different reaction mechanisms, once sorted in excitation energy bins, lead to comparable partitions (except an increased secondary fission probability for the residue formed in the heaviest source) strongly pleads for a thermal equilibrium. If we consider a thermal scenario, critical-like behaviours have been theoretically observed in finite systems also inside the coexistence region [11–14,30] and at supercritical densities [7]; one may then wonder whether power laws are connected to phase transitions altogether. Because of the apparent universality of this phenomenon we cannot a-priori exclude that some peculiar non critical models lead to power laws, critical-like exponents and Fisher scaling. In this respect it is interesting to remark that if Fisher scaling is applied to the Gemini model (that does not contain any phase transition) in an excitation energy range from 1 to 8 A MeV (that includes the apparent critical energy extracted from data) a critical phenomenon can be excluded. The fit of the size distribution gives different solutions, depending on the constraints imposed on τ. Under the constraint $2 < \tau < 3$ [45], τ is found at its allowed lower limit 2 and E_c^* is found at its upper allowed value 15 A MeV. When τ is let to vary freely, the best fit is obtained for $\tau = 1.5$ and $E_c^* = 7.7$ A MeV. Both solutions are not compatible with an equilibrium phase transition, and indicate that the charge distribution never passes through a power law ($\Delta\mu \neq 0$). In both cases the quality of the fit is good ($\chi^2 \approx 1$), meaning once again that the observation of a linear behaviour of the scaled distributions over several orders of magnitude is not in itself a proof of a critical behavior.

4.5. Source size effects on scaling

To check whether the scaling function Eqs. (2)–(4) is able to describe the decay of finite charged nuclear matter, with parameters independent of the size of the source, a subset of events of equal statistics has been selected for the four sets of central events (1000 events

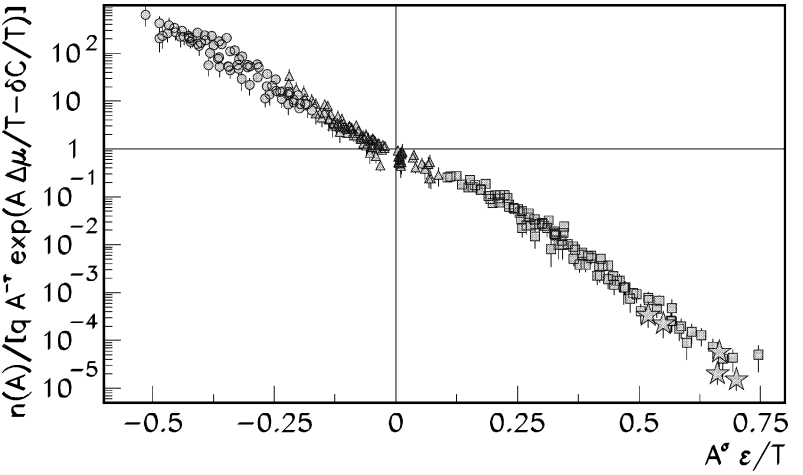

Fig. 11. Simultaneous fit of an equal statistics subsample of the central events with the scaling function ansatz Eqs. (2)–(4). Symbols as in Fig. 6.

for each reaction) and the Fisher scaling has been repeated on this sample (over 270 data points).

The resulting scaling function is displayed in Fig. 11 and the parameters are reported in Table 4 (label: 'All central'). The reasonably good quality of the scaling and the agreement of the critical-like parameters with the results shown in Table 1 and 2 strongly support the universality of the scaling: the critical-like behavior and the whole shape of the scaling function are independent both on the size of the system and on the entrance channel. This implies that the determination of the critical-like parameters is robust with respect to the possible effects induced by the Coulomb interaction and by the reaction mechanism.

5. Summary and conclusions

The decay of the quasi-projectile formed in peripheral 35 A MeV Au + Au collisions has been compared with different sets of central events in terms of scaling analysis and critical-like behaviors.

All reactions show a critical-like behaviour at an excitation energy of about 4.5 A MeV, with critical-like exponents $\tau \approx 2.1$, $\sigma \approx 0.66$. Analyzing the velocity correlations between the two heaviest fragments we have demonstrated that fission is an important deexcitation channel for the secondary decay of heavily charged systems. If this decay is back-traced we observe a good scaling with the size of the source between the peripheral QP events ($Z_{\text{source}} \approx 80$) and the central Au + Cu ones ($Z_{\text{source}} \approx 100$).

However, the quality of the scaling and the compatibility of central and peripheral collisions, even if impressive, do not demonstrate unambiguously the existence of a transition, neither its thermal nature nor its order. Indeed, the shape of the scaling function (i.e., the parameters c_0 and $\Delta\mu$) strongly depends on the technical assumptions made in the fit procedure. Moreover, a similar scaling is obtained with the ansatz Eq. (1) that has been

introduced in the context of percolation, for which an equation of state is not a relevant concept.

Scaling analyses have thus to be considered mainly as a way to test the reducibility of an ensemble of data to a scaling function and to a few scaling parameters, i.e., a tool to handle the data and not a proof of a specific fragmentation scenario.

Though the parameters of the fit do not allow to extract direct information on the equation of state of nuclear matter still a universal scaling behavior for the fragmentation pattern of different sources, produced within different entrance channel mechanisms, around a point of well defined excitation energy, strongly suggests a thermally driven phenomenon [44].

If in a thermal process the distributions behave like a power law for a specific value of the control parameter (energy or temperature), this indeed points in the direction of a scale invariance and the fragmentation can then be considered as a critical(-like) phenomenon. This restricts a little more the possible origin of fragment production. In particular, this behavior is expected in thermal models with a second order phase transition [11–13,30]. However, even in these models a critical behavior is not directly related to the thermodynamical critical point. Indeed, a good scaling and critical-like behavior of the mass distribution can be found inside the coexistence region if the system is small enough [11,13,30]. In particular in macroscopic statistical models like SMM the topologic term $-\tau \ln A$ is not included in the free energy, while power laws are systematically observed inside the coexistence region [22,28]. This illustrates that pseudo-critical behaviors can be simulated by finite size effects.

One should, therefore, distinguish three independent observations: a scaling of the size distribution, a critical-like behavior related to a scale invariance, and a possible second order phase transition at a thermodynamical critical point. While the two first observations can be tested through the scaling analysis of size distribution, the possible link with thermodynamics requires independent information directly related to the occurrence of a phase transition.

Concerning the Au QP events, the analysis of fluctuations [9] rather point to a phase coexistence and a first order phase transition. In this respect it is interesting to note that experimentally power laws occur at the same excitation energy as the maximum of fluctuations of the configurational energy [9]. In thermal models fluctuations pass through a maximum at all densities [46], including the subcritical regime. If fluctuations are sufficiently large so that the correlation length becomes comparable to the size of the system, this could have, in finite system, the same effect as a diverging correlation length at the thermodynamical limit, i.e., an critical-like behavior. Further work to experimentally assess this point is in progress [47].

Acknowledgements

The authors would like to acknowledge the Multics-Miniball Collaboration, which has performed the experiments. The authors are also grateful to P.F. Mastinu and P.M. Milazzo for a critical reading of the manuscript.

This work has been partially supported by NATO grants CLG-976861 and by grants of Italian Ministry of Instruction, University and Research (MIUR) and Alma Mater Studiorum (Bologna University).

References

[1] J.E. Finn, et al., Phys. Rev. Lett. 49 (1982) 1321;
A.S. Hirsch, et al., Nucl. Phys. A 418 (1984) 267;
M. Mahi, et al., Phys. Rev. Lett. 60 (1988) 1936;
A.D. Panagiotou, M.W. Curtin, H. Toki, D.K. Scott, P.J. Siemens, Phys. Rev. Lett. 52 (1984) 496.
[2] X. Campi, J. Desbois, E. Lipparini, Phys. Lett. B 138 (1984) 353.
[3] M.L. Gilkes, et al., Phys. Rev. Lett. 73 (1994) 1590;
J.B. Elliott, et al., Phys. Rev. C 49 (1994) 3185;
J.B. Elliott, et al., Phys. Lett. B 418 (1998) 34;
J.A. Hauger, et al., Phys. Rev. C 57 (1998) 764;
R.P. Scharenberg, et al., Phys. Rev. C 64 (2001) 054602.
[4] M. D'Agostino, et al., Nucl. Phys. A 650 (1999) 329.
[5] G.F. Bertsch, P.J. Siemens, Phys. Lett. B 126 (1983) 9.
[6] X. Campi, Phys. Lett. B 208 (1988) 351;
X. Campi, H. Krivine, Z. Phys. A 344 (1992) 81.
[7] X. Campi, H. Krivine, N. Sator, Nucl. Phys. A 681 (2001) 458.
[8] J. Pochodzalla, et al., Phys. Rev. Lett. 75 (1995) 1040.
[9] M. D'Agostino, et al., Phys. Lett. B 473 (2000) 219;
M. D'Agostino, et al., Nucl. Phys. A 699 (2002) 795.
[10] J.B. Natowitz, et al., Phys. Rev. C 65 (2002) 34618.
[11] F. Gulminelli, Ph. Chomaz, Phys. Rev. Lett. 82 (1999) 1402;
F. Gulminelli, Ph. Chomaz, Int. J. Mod. Phys. E 8 (1999) 1.
[12] C.B. Das, S. Das Gupta, A. Majumder, Phys. Rev. C 65 (2002) 34608;
C.B. Das, et al., Phys. Rev. C 66 (2002) 044602.
[13] J.M. Carmona, J. Richert, P. Wagner, Phys. Lett. B 531 (2002) 71.
[14] A.H. Raduta, et al., Phys. Rev. C 65 (2002) 034606.
[15] J.B. Elliott, et al., Phys. Rev. Lett. 88 (2002) 042701, nucl-ex/0104013;
J.B. Elliott, et al., nucl-ex/0205004.
[16] C. Williams, et al., . Phys. Rev. C 55 (1997) R2132;
J.B. Elliott, et al., Phys. Rev. C 59 (1999) 550;
C. Williams, et al., Phys. Rev. C 59 (1999) 552.
[17] M. D'Agostino, et al., Phys. Rev. Lett. 75 (1995) 4373.
[18] M.F. Rivet, et al., Phys. Lett. B 430 (1998) 217.
[19] D. Stauffer, A. Aharony, Introduction to Percolation Theory, Taylor and Francis, London, 1992.
[20] I. Iori, et al., Nucl. Instrum. Methods A 325 (1993) 458.
[21] R.T. DeSouza, et al., Nucl. Instrum. Methods A 295 (1990) 109.
[22] J.P. Bondorf, A.S. Botvina, A.S. Iljinov, I.N. Mishustin, K. Sneppen, Phys. Rep. 257 (1995) 133.
[23] P.M. Milazzo, et al., Phys. Rev. C 58 (1998) 953.
[24] J.L. Cardy (Ed.), Finite Size Scaling, North-Holland, Amsterdam, 1988.
[25] J.B. Elliott, et al., Phys. Rev. C 62 (2000) 064603.
[26] M.E. Fisher, Physics 3 (1967) 255.
[27] J.A. Lopez, C.O. Dorso, Phase Transformations in Nuclear Matter, World Scientific, Singapore, 2000.
[28] K.A. Bugaev, M.I. Gorenstein, I.N. Mishustin, W. Greiner, Phys. Rev. C 62 (2000) 044320;
K.A. Bugaev, M.I. Gorenstein, I.N. Mishustin, W. Greiner, Phys. Lett. B 498 (2001) 144.
[29] M. Belkacem, V. Latora, A. Bonasera, Phys. Rev. C 52 (1995) 271.
[30] F. Gulminelli, et al., Phys. Rev. C 65 (2002) 51601.
[31] J.F. Lecolley, et al., Nucl. Instrum. Methods A 441 (2000) 517.

[32] R.J. Charity, et al., Nucl. Phys. A 483 (1988) 371.
[33] M. D'Agostino, et al., Phys. Lett. B 371 (1996) 175.
[34] P. Desesquelles, et al., Nucl. Phys. A 633 (1998) 547.
[35] P.M. Milazzo, et al., Phys. Rev. C 66 (2002) 021601(R).
[36] A.J. Cole, Phys. Rev. C 65 (2002) 031601.
[37] A.J. Cole, Statistical Models for Nuclear Decay, Fundamental and Applied Nuclear Physics Series, IOP, 2000, pp. 243–246.
[38] Y.D. Kim, et al., Phys. Rev. C 45 (1992) 338;
Y.D. Kim, et al., Phys. Rev. C 45 (1992) 387;
T. Glasmacher, et al., Phys. Rev. C 50 (1994) 952.
[39] R. Trockel, et al., Phys. Rev. Lett. 59 (1987) 2844;
M.A. Lisa, W.G. Gong, C.K. Gelbke, W.G. Lynch, Phys. Rev. C 44 (1991) 2865.
[40] M. D'Agostino, et al., Phys. Lett. B 368 (1996) 259.
[41] T. Glasmacher, et al., Phys. Rev. C 51 (1995) 3489.
[42] C.O. Dorso, J.A. Lopez, Phys. Rev. C 64 (2001) 027602.
[43] H.R. Jaqaman, D.H.E. Gross, Nucl. Phys. A 524 (1991) 321.
[44] L.G. Moretto, et al., Nucl. Phys. A 681 (2001) 239.
[45] A. Bonasera, M. Bruno, C. Dorso, P.F. Mastinu, Critical phenomena in nuclear fragmentation, Riv. Nuovo Cimento 23 (2) (2000).
[46] Ph. Chomaz, F. Gulminelli, Nucl. Phys. A 647 (1999) 153.
[47] M. D'Agostino et al., in preparation.